JMEPEG (2009) 18:575–581
DOI: 10.1007/s11665-009-9474-y

1059-9495/$19.00

Influence of Carbon on the Microstructure of a Fe-Mn-Si-Cr-Ni Alloy

Khaled M. Mostafa, J. De Baerdemaeker, N. Van Caenegem, D. Segers, and Y. Houbaert

(Submitted August 21, 2008; in revised form April 28, 2009)

The influence of the addition of C to the Fe-Mn-Si-Cr-Ni base material is investigated at room temperature. Steel samples were deformed during a tensile experiment up to a strain of 17%. Light optical microscopy (OM) and x-ray diffraction (XRD) gave information about the different micro-structural phases that exist in the deformed and the undeformed alloys. The evolution of the defect structure is followed by positron annihilation techniques such as Doppler broadening of annihilation radiation spectroscopy (DBAR) and the positron annihilation lifetime spectroscopy (PALS). During deformation a martensitic ε-phase is induced. The size of the martensite plates increases with increasing deformation.

Keywords nondestructive testing, optical microscopy, shape memory alloys

1. Introduction

Fe-Mn alloys with 10-30% Mn are characterized by the reversible and self-accommodating face centred cubic (fcc) γ austenite to hexagonal close packed (hcp) ε martensite transformation (Ref 1). Ferrous shape memory alloys (SMA) based on Fe-Mn alloy system have received much attention since the eighties of the last century and there are definite signals from the shape memory materials research community that they may become a new class of one-way SMAs of great technical importance due to their cost-effectiveness (Ref 2). The shape memory effect (SME) in FeMnSi alloys was first reported by Sato et al. (Ref 3). They have found that a single crystal of a Fe-30%Mn-1%Si alloy exhibited a complete SME when deformed in the ⟨414⟩ direction. Sato et al. (Ref 4) and Murakami et al. (Ref 5) also succeeded in developing poly-crystalline FeMnSi SMAs. Moriya et al. (Ref 6) and Otsuka et al. (Ref 2) developed FeCrNiMnSi and FeCrNiMnSiCo SMAs, which are characterized by their corrosion resistance.

This article is an invited paper selected from presentations at Shape Memory and Superelastic Technologies 2008, held September 21-25, 2008, in Stresa, Italy, and has been expanded from the original presentation.

Khaled M. Mostafa, Department of Subatomic and Radiation Physics, Ghent University, Proeftuinstraat 86, B-9000 Ghent, Belgium and Department of Metallurgy and Materials Science, Ghent University, Technologiepark 903, B-9052 Ghent, Belgium, and **J. De Baerdemaeker** and **D. Segers**, Department of Subatomic and Radiation Physics, Ghent University, Proeftuinstraat 86, B-9000 Ghent, Belgium; and **N. Van Caenegem** and **Y. Houbaert**, Department of Metallurgy and Materials Science, Ghent University, Technologiepark 903, B-9052 Ghent, Belgium. Contact e-mail: khaled.mostafa@ugent.be.

The large hysteresis and a poor shape recovery in the Fe-Mn binary system was addressed by making specific alloying additions of Si, C, Co, Ni, and Cr. The SME in FeMnSi alloys strongly depends on the alloy composition. The addition of C strengthens the austenite and increases the stacking fault energy (Ref 7, 8), while it decreases the Ms temperature (Ref 9, 10). Tian et al. (Ref 11) determined the effect of carbon on the Ms of FeMnAlCr alloy and suggested that C strongly depresses the $\gamma \rightarrow \varepsilon$ martensitic transformation. Tsuzaki et al. (Ref 9) examined the effect of carbon in the FeMnSi alloy. They reported that the SME is improved by the addition of carbon.

In order to reach a complete SME, three conditions must be fulfilled. First, the deformation must result in the stress-induced ε martensite formation only. Second, the yield stress of the γ matrix should be as high as possible to avoid an initial deformation by slip. Finally, the shape strain of stress-induced martensite should be completely reversible, which means that the martensite interface must remain mobile at all times. The forward and reverse transformations occur by the movement of planar martensite interfaces, which contain the transformation dislocations. The required martensite morphology for ferrous SMA is of the thin plate type.

Because the SMAs posses low stacking faults energy, the nucleation of the martensite may occur by means of the stacking fault mechanism (Ref 12). The transformation results in thin ε martensite plates, which have specific crystallographic orientations with respect to each other. This is due to the fact that the martensitic $\gamma \rightarrow \varepsilon$ transformation is obtained by the glide of isolated Shockley partial dislocations on every second $\{111\}_\gamma$ plane. There is no macroscopic deformation of the single crystal when the $\gamma \rightarrow \varepsilon$ transformation is induced thermally. The deformation results in the dominance of ε martensite variants, which are suitably oriented with respect to the applied stresses, and a decrease of the volume fraction of the other ε variants in each original γ grain. It must be mentioned that FeMnSi-type ferrous SMAs always contain retained austenite at room temperature. The ε martensite forms dense regions of transformed regions, which still contain the parent γ phase. At the intersection of two variants of ε martensite, α′ martensite was often observed (Ref 13). It is very likely that the formation of α′ martensite is the main

cause for relatively low recovery of the ferrous SMAs. The α′ regions impede the reverse motion of the Shockley partial dislocations. One of the challenging problems of the Fe-Mn-based alloys is the relatively low, fully reversible pre-strain, usually less than 2% in contrast to over 6% in the Ni-Ti and Cu-based alloys.

During the last few years, the positron annihilation technique has been widely used to study defects and phase transition in SMAs. Most of the work had been done on the Ni-Ti and Cu-based alloys (Ref 14-16). Very few publications have been published about the Fe-Mn-based alloys (Ref 17, 18).

In the present study, the influence of deformation and carbon addition on Fe-Mn-Si-Cr-Ni alloys is studied by a combination of optical microscopy (OM), x-ray diffraction (XRD), and positron annihilation spectroscopy (PAS) techniques. OM and XRD give accurate information on the different phases present in the material. PAS techniques were used to study the defect behavior in the samples and to see if any effect of the phase transformation during deformation could be detected.

The positron annihilation technique is known to be a highly sensitive method for open volume defects (Ref 19). The defect structure after plastic deformation of metallic samples can also be investigated with the positron annihilation technique (Ref 20). It is expected that PAS can help in understanding more about the stress-induced martensitic transformation in FeMn-based alloys. Two basic techniques are used: positron annihilation lifetime spectroscopy (PALS) and Doppler broadening of annihilation radiation spectroscopy (DBAR).

Positrons from a radioactive source are injected into the sample. After thermalization, the positron diffuses through the solid and gets trapped by defects present in the sample. Defects capable of localizing the positron are vacancies, vacancy agglomerates, voids and dislocations. PAS has proven to be a uniquely sensitive probe for nanometre defects. The high sensitivity of positrons to defects stems from two facts: their attraction to atomic-size defects and their long diffusion length, which is about a few hundred nanometres in most materials (Ref 21). PALS can quantify the size of open volume defects as well as the defect concentration and is based on the precise measurement of the lifetime of a positron in a solid. The concentration can be deduced from the fraction of positrons that annihilate from a trapped state. The defect size is directly related to the position lifetime; the larger the defect, the lower the local electron density is and consequently the longer the positron lifetime will be (Ref 22).

DBAR is based on the measurement of the linear momentum of the annihilating electron-positron pair. The photons created during the electron-positron annihilation are detected by a germanium detector. The shape of the resulting photo-peak reflects the momentum distribution of the original electron-positron pair. This distribution is determined by the size and the nature of the defects. Measurements of the Doppler broadening of positron-electron annihilation radiation are generally characterized by the S (shape) parameter, defined as the ratio between the central part of the annihilation spectra and the total spectra. This parameter reflects the positron annihilation with valence electrons (low momentum). In general, a high value of S indicates positron annihilation in open volume defects. A second useful parameter for the analysis of DBAR is the W (wing) parameter, which reflects the positron annihilation with high momentum electrons (core electrons). It is defined as the ratio of counts in two side windows and the total number of counts.

The plastic deformation of metals and alloys produces changes in the density and distribution of defects. In plastic deformed metals and alloys, the positrons are captured by dislocations and vacancies. In polycrystalline samples, the deformation becomes complex due to the various interactions between dislocations and the grain boundaries (Ref 23). The interaction of dislocations during the deformation can lead to a raise of the formation of jogs and point defects. Some measurements of positron annihilation have been made for martensitic transformations in metals and alloys (Ref 24-27). Dislocations produced during the transformation must be considered when martensitic transformation is studied by positron annihilation. Segers et al. studied together different types of SMAs (Ref 17, 28, 29).

2. Experimental

Two different Fe-Mn-Si-Cr-Ni alloys were prepared for this study. Their chemical composition is given in Table 1. They were cast in an air furnace, air cooled, reheated to 1200 °C and hot rolled on a laboratory mill from 20 to 2 mm and air cooled. In order to austenitize the samples; they were heated to 1100 °C for 15 min and water quenched to room temperature. The specimens examined by optical microscopy were first mechanically polished and then electrolytically polished in a solution of 20% perchloric acid and 80% butylcellosolve. Afterwards, the specimens were color etched in an aqueous solution of 1.2% $K_2S_2O_5$ and 0.5% NH_4HF_2. Each phase could clearly be distinguished on the basis of its color and morphology.

Positron lifetime measurements were performed at room temperature using a fast-fast lifetime spectrometer. Each spectrum contained at least 10^6 counts and was analyzed with the program LT by Kansy (Ref 30). As a positron source ^{22}NaCl of about 10 μCi was sealed between two kapton foils with a thickness of 7.5 μm, which had to be surrounded by two identical samples in the so-called sandwich configuration (Ref 31). The resolution of the setup is 200 ps, while the source contribution was 14% with a single lifetime of 384 ps.

The tensile tests were carried out on LRX–PLUS (LLOYD Instruments) tensile test machine with maximum force of 5 kN. The shape and dimensions of the specimens are shown in Fig. 1. Tensile test was performed to make elongation of the sample. The elongation rate was 0.1 mm/min. During the deformation of the sample, the Doppler broadening (DB) of the 511 keV annihilation line is measured using high-purity germanium detector with a resolution of 1.2 keV at the 514 keV line of ^{85}Sr. The results are analyzed in terms of the so-called *S*- and *W*-parameter. The *S* parameter is obtained for each sample from the measured 511-keV peak by dividing the counts in the central region by the total counts in the peak after subtracting background. The energy window of the central

Table 1 Chemical composition of Fe-Mn-Si-Cr-Ni-C in wt.%

Element	Fe	Mn	Si	Cr	Ni	C
FeMnSiCrNi	67.34	12.6	6	9.27	4.74	0.05
FeMnSiCrNiC	66.84	12.56	6.09	9.44	4.89	0.18

region was chosen so that *S* parameter equals to 0.5 in the well-annealed Fe sample.

3. Results and Discussion

3.1 OM and XRD

Figure 2 shows the microstructure of the Fe-Mn-Si-Cr-Ni-C alloys before and after deformation. The micro-structural analysis for the undeformed samples revealed the presence of large austenite grains (γ phase), residual ferrite grains and ε phase. The amount of residual ferrite grains between the austenite is less in the alloy without carbon.

This is also measured with the XRD (Fig. 3). The ε martensite is clearly visible in the alloy without carbon and is less in the carbon alloyed one. It appears as thin parallel lines with dark contrast inside the austenite grains. This small quantity of ε martensite before the deformation process is probably induced during grinding or polishing or can be induced thermally. By deformation, more ε martensite is

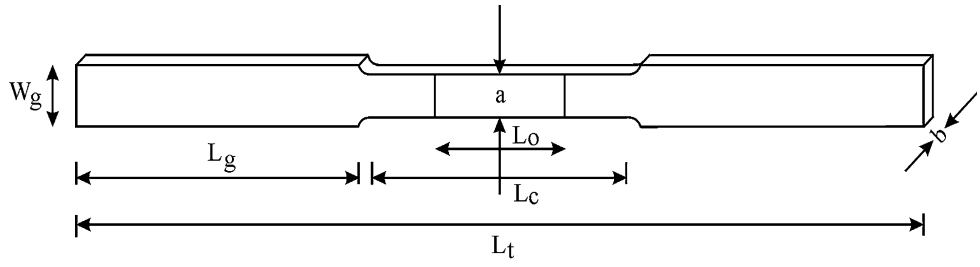

Specimen type	a	L_t	Wg	Lg	L_c	L_o	b
FeMn	7	150	10	50	45	23	1

Dimensions in mm

Fig. 1 Shape and dimensions of the tensile test sample

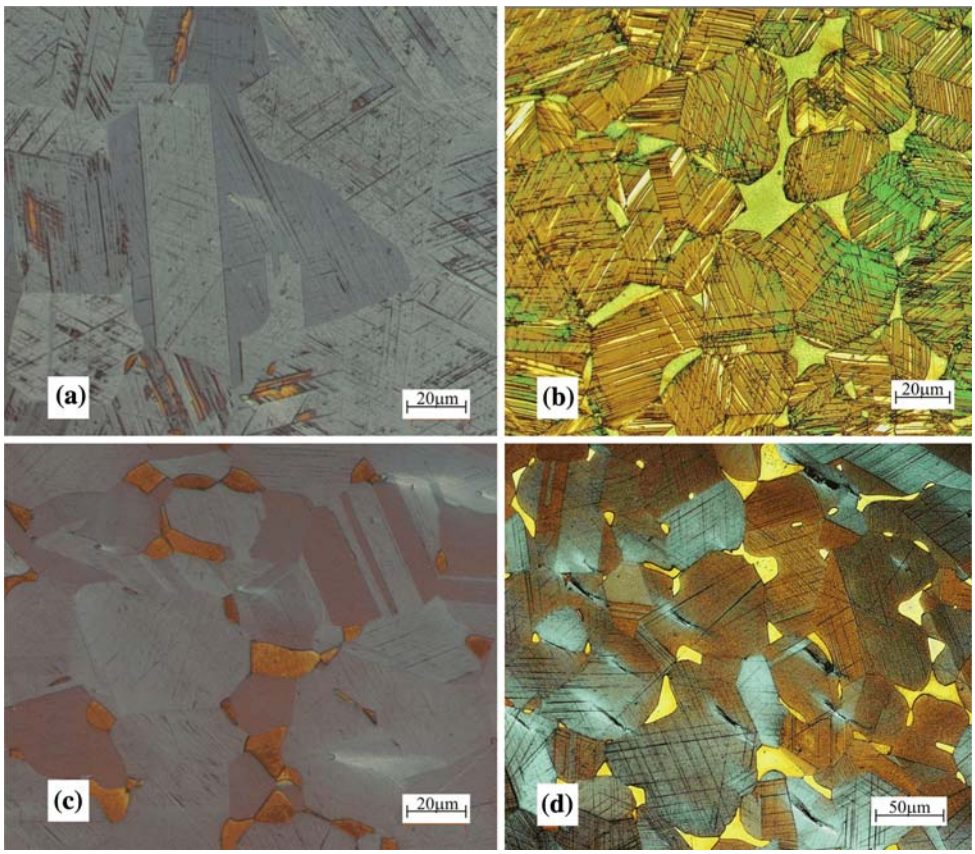

Fig. 2 Light optical microstructures (OM) for the alloys: (a) Fe-Mn-Si-Cr-Ni undeformed, (b) deformed, (c) Fe-Mn-Si-Cr-Ni-C undeformed, and (d) deformed

transformed from the austenite. There is an increase in the intensity of the $(002)_\varepsilon$ peak. In the OM, the ε phase appears as broader white lines in the alloy without carbon and clearly thinner black lines in the alloy with carbon. From the XRD result we can also conclude that the alloy without carbon contains more ε martensite phase.

Comparing the deformed and the non-deformed samples through the OM pictures, one can see that the stress induced

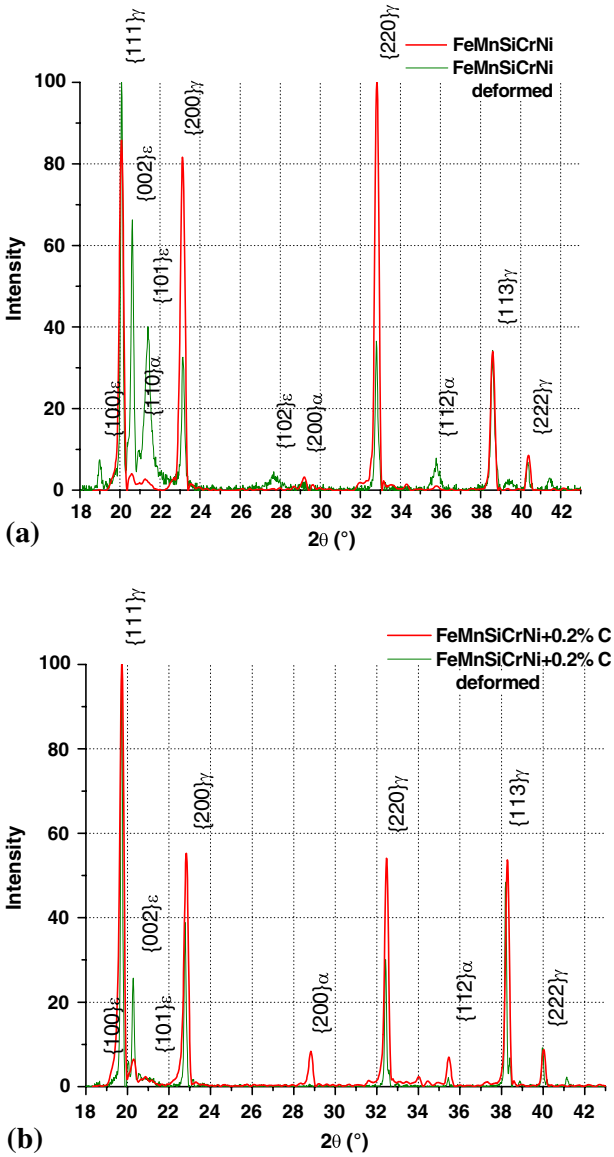

Fig. 3 XRD for the alloys: (a) undeformed and deformed Fe-Mn-Si-Cr-Ni; (b) undeformed and deformed Fe-Mn-Si-Cr-Ni-C

$\gamma \rightarrow \varepsilon$ transformation proceeds by the growth and broadening of the existing ε martensite plates rather than the formation of new plates (Ref 32, 33).

3.2 Positron Annihilation

Positron annihilation lifetime data are presented in Table 2. For the undeformed samples of Fe-Mn-Si-Cr-Ni-C, the lifetime for positrons was 107 ps which is the same in case of defect-free Fe (Ref 34). In the widely used two-state trapping model (Ref 35), it is assumed that positrons annihilate either in the bulk portion or get trapped in defects before annihilation. In the latter case, they survive for more time in the material, which is given by the longer lifetime. This variation of the lifetime values is relevant to defect type (dislocation, mono-vacancy, cluster of vacancy, micro-void). In pure Fe, the lifetime value for positrons trapped in dislocations is around 160 ps and for positrons trapped in mono-vacancies, it is around 180 ps (Ref 36-39).

For the deformed samples, the positron annihilation lifetime spectra have two components for the lifetime. The shortest lifetime components τ_1 for the two samples are 61 and 67 ps, which are due to the annihilation of non-trapped positrons. The second lifetime component for the two samples is 151 and 150 ps, which are related to the positron annihilation in dislocations. The concentrations of dislocations in both deformed samples are calculated using the same equations and parameters used by Park et al. (Ref 40). One can conclude that the alloy without carbon has more dislocations than the one of carbon.

3.3 Doppler Broadening (DB) and Stress-Strain Relation

There are different stages of deformation of the SMAs, which have different deformation mechanisms. The first stage happens in the range of smaller strains, the self-accommodation mechanism of martensite plates, not the dislocation slip mechanism, is responsible for the deformation of the SMAs. The orientations of martensite plates are adjusted or reoriented in accordance with the direction of the applied stress, which results in macroscopic deformation, but does not result in an increase of micro defects. Even if defects as twin boundaries and stacking faults may be created during deformation, they are thought to be unable to attract positrons. Once the strain increases beyond several percent, another deformation mechanism will take place. Dislocation slip produces many defects, capable to trap the positrons. The S parameter can be written as

$$S = \sum_i P_i S_i + \sum_i P_{d_i} S_{d_i}$$

where P_i is the probability of the annihilation of positrons in phase i and S_i is the respective line shape parameter. S_{d_i} counts for the part of positrons annihilated due to the defects

Table 2 Positron annihilation lifetime in Fe-Mn-Si-Cr-Ni-C samples

Sample	τ_1, ps	I_1, %	τ_2, ps	I_2, %	Concentration of dislocations, 10^{14} m^{-2}
FeMnSiCrNi	107	100	…	…	
FeMnSiCrNi 15% deformed	61	21	151	79	1.287
FeMnSiCrNiC	107	100	…	…	
FeMnSiCrNiC 15% deformed	67	24	150	76	1.046

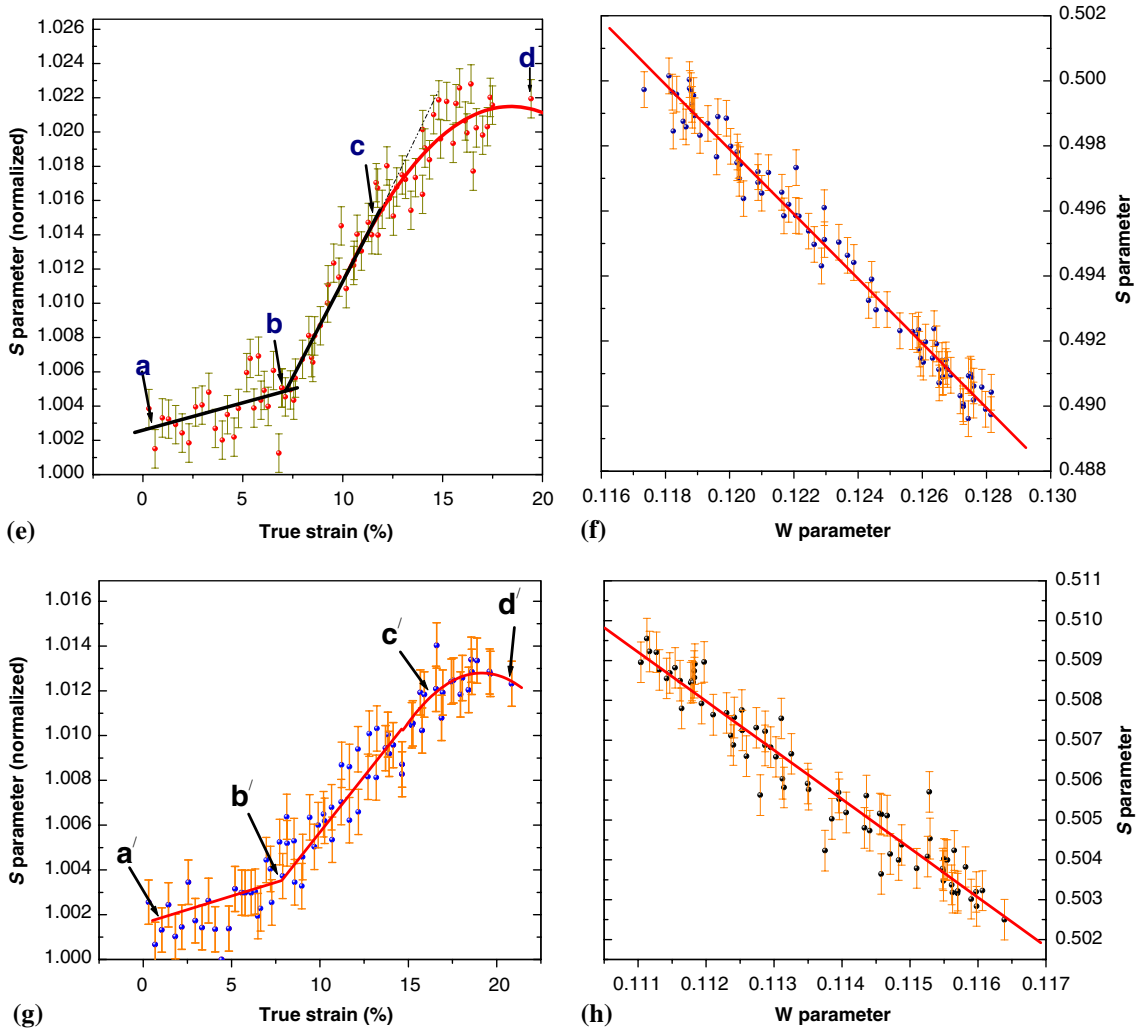

Fig. 4 Plot of *S* parameter (normalized to the *S* values of the corresponding un-deformed samples) as function of strain for (e) FeMnSiCrNi and (g) FeMnSiCrNiC alloys and the *S*-*W* relation for (f) FeMnSiCrNi and (h) for FeMnSiCrNiC alloys

of phase *i* with its respective probability P_{d_i} (Ref 17). In Fig. 4 as the degree of deformation is smaller than 5%, the change in *S* parameter (normalized to the *S* values of the corresponding un-deformed samples) is very small to be recognized and for deformations higher than 5% the *S* parameters increase remarkably. An increase of defect density leads to an increase of the *S*-parameter in both samples, which can be recognized through the comparison of the data of the deformed and the undeformed samples. For the common metals and alloys, the positron parameters increase markedly at the early stage of increasing strain, and rapidly became saturate when the samples are subjected to plastic deformation (Ref 41-43).

3.3.1 Effect of Carbon on the *S* Parameter. In both samples (low carbon, high C sample) the pattern of the *S* parameter (normalized to the *S* values of the corresponding un-deformed samples) versus the deformation gave the *S*-line shape curve (Fig. 4e, g). At the first stage increasing the true strain up to 7% (a $\rightarrow$ b) and (a′ $\rightarrow$ b′) respectively leads to a slight increase in the value of the *S* parameter. The next stage is starting from 7% up to 11% (b $\rightarrow$ c) in case of the low C sample and between 7% and 16% (b′ $\rightarrow$ c′) of the high C sample. The value of *S* parameter increases greatly with increasing strain. This is also observed in CuZnAl SMAs (Ref 16). The behavior of the *S* parameter in case of the high carbon sample differs from that of the low carbon sample. The *S* parameter increases with increasing strain but the change in the *S* parameter is not that high as the one of the low carbon sample. This means that the carbon content added to the alloy has an effect in the change of the microstructure, the concentration, and the type of defects created in the alloys.

During deformation the transformation $\gamma \rightarrow \varepsilon$ proceeds and α' martensite is formed at the intersections of the ε plates, which causes strain hardening. As shown by the XRD measurement, the low carbon alloy forms much more ε martensite during deformation, which results in a higher strain hardening compared to the high C alloy. The uniform elongation is larger for low C alloy. This might be correlated with the fact that due to the formation of the ε phase or twinning the microstructure is progressively subdivided in much smaller sized units in the C-added alloy. Consequently, the effective grain size is reduced. In such steels with a smaller grain size, more stress is needed for the movement and multiplication of dislocations. They are impeded by the grain

boundaries, which lead to a lower strain hardening and a smaller uniform elongation. This can be recognized in the behavior of the *S* parameter in both samples. The *S* parameter increases with increasing deformation and in case of low carbon steel, it is clear that the change in the *S* parameter is more than the one of high C sample.

From the *S-W* plots (Fig. 4f, h), the relation is giving one straight line (lines are drawn as a guide for the eyes). This can be ascribed to the existence of one kind of defect. This defect could be dislocations, which is correlated with lifetime results.

4. Conclusion

From the results of the positron annihilation, the Doppler broadening parameter *S* increases as a result of the trapping of positrons in defects. In the early stages of deformation, no significant increases of the *S* parameters for both alloys are observed. The increase of *S* is caused by an increasing number of lattice defects (dislocations). The carbon content in the alloys has a significant effect in the value of the *S* parameter, which means the concentration of defects.

References

1. T. Maki, *Shape Memory Materials*, K. Otsuka and C.M. Wayman, Ed., Cambridge University Press, UK, 1998, p 117–132
2. H. Otsuka, H. Yamada, T. Maruyama, H. Tanahashi, S. Matsuda, and M. Murakami, Effects of Alloying Additions on Fe-Mn-Si Shape Memory Alloys, *Trans. ISIJ*, 1990, **30**, p 674
3. A. Sato, E. Chishima, K. Soma, and T. Mori, Shape Memory Effect in $\gamma \rightarrow \varepsilon$ Transformation in Fe-30Mn-1Si Alloy Single Crystals, *Acta Metall.*, 1982, **30**, p 1177
4. A. Sato, Y. Yamaji, and T. Mori, Physical Properties Controlling Shape Memory Effect in FeMnSi Alloys, *Acta Metall.*, 1986, **34**, p 287
5. M. Murakami, H. Otsuka, H.G. Suzuki, and S. Matsuda, Complete Shape Memory Effect in Polycrystalline Fe-Mn-Si Alloys, *Proceeding of the International Conference on Martensitic transformations (ICOMAT-86)*, Japan Institute of Metals, 1986, p 985
6. Y. Moriya, T. Sampei, and I. Kozasu, Annual Meeting at Yokohama, *Conference Abstract of Spring Meeting of JIM*, 1989, p 222
7. L.M. Kaputkina and V.G. Prokoshkina, Martensitic Transformations Structure and Strengthness of Processed High-Nitrogen and High-Carbon Ferrous Alloys, *J. Phys. IV Fr.*, 2003, **112**, p 263
8. D. Dulieu and J. Nutting, Metallurgical Development in High Alloy Steels, *Iron Steel Inst.*, 1964, **86**, p 82
9. K. Tsuzaki, Y. Natsume, Y. Tomota, and T. Maki, Effect of Solution Hardening on the Shape Memory Effect of FeMn Based Alloys, *Scr. Metall. Mater.*, 1995, **33**, p 1087
10. P. Dai, Effect of Solution Hardening on the Shape Memory Properties of Fe-Mn-Si Based Alloys, *J. Mater. Sci. Lett.*, 2000, **19**, p 111
11. X. Tian, Y.S. Zhang, and C.X. Shi, Relationship Between $\gamma \rightarrow \varepsilon$ Transformation Temperature $M_{\varepsilon S}$ and Composition of Metastable Austenitic Region in Fe-Mn-Al-Cr System, *Acta Metall. Sinica*, 1986, **22**, p A101 (in Chinese)
12. H. Inagaki, Shape Memory Effect of Fe-14% Mn-6% Si-9% Cr-6% Ni Alloy Polycrystals, *Z. Metallkd.*, 1992, **83**, p 90
13. G.J. Arruda, V.T.L. Buono, and M.S. Andrade, The Influence of Deformation on the Microstructure and Transformation Temperatures of Fe-Mn-Si-Cr-Ni Shape Memory Alloys, *J. Mater. Sci. Eng.*, 1999, **272–275**, p 528
14. I. Hurtado, D. Segers, L. Dorikens-Vanpraet, C. Dauwe, and J. Van Humbeeck, Positron Annihilation Measurements in Cu-Al-Ni Based Shape Memory Alloys, *J. Phys. IV Colloq.*, 1995, **C8**, p 949
15. I. Hurtado, D. Segers, J. Van Humbeeck, L. Dorikens-Vanpraet, and C. Dauwe, Evolution of the Positron Annihilation Lifetime for Ageing in Beta-Phase Cu-Al-Ni-(Ti)-(Mn) Shape Memory Alloys, *Scr. Metall.*, 1995, **33–35**, p 741
16. W. Jing-cheng, S. Zi-chang, and Z. Hao, An Anomaly of the Parameters of Positron Annihilation for Plastically Deforming Shape Memory Alloys, *J. Scr. Metall. Mater.*, 1990, **24**, p 1511
17. J. Van Humbeeck, G. Ghosh, L. Delaey, D. Segers, M. Dorikens, and L. Dorikens Vanpraet, Defect Accumulation During the Martensitic Transformation in Fe-Mn-Ni Shape Memory Alloys, Positron Annihilation, *Proceeding of the ICPA8 Conference*, 1989, p 395
18. T. Liu, R.D. Xia, G.W. Liu, Z.T. Zhao, R.Z. Ma, W.H. Wang, and Y.H. Guo, A Positron Annihilation Study of Stress-Induced Martensite Transformation in Fe-Mn Based Alloys, *J. Mater. Sci. Lett.*, 1998, **17**, p 887
19. P. Hautojarvi, A. Vehanen, A. Dupasquier, M.J. Manninen, P.E. Mijnarends, R.M. Nieminen, and R.N. West, *Positrons in Solid*, Springer-Verlag, Berlin, 1979, p 1–23
20. K. Petersen, *Proceedings of the "Enrico Fermi"*, W. Brandt, Ed., International School of Physics, 1983, p 298
21. R. Krause-Rehberg and H.S. Leipner, *Positron Annihilation in Semiconductors*, Springer, Berlin, 1999
22. P. Hautojarvi, J. Heinio, M. Mannien, and R. Nieminen, The Effect of Microvoid Size on Positron Annihilation Characteristics and Residual Resistivity in Metals, *Philos. Mag.*, 1977, **35**, p 973
23. C. Hidalgo, S. Linderoth, and N. de Diego, The Recovery of Deformed Zinc Studied by Positron Annihilation Spectroscopy, *Philos. Mag.*, 1986, **A64**, p L61
24. T.D. Troev, K. Hinode, S. Tanigawa, and M. Doyama, Positron Study of the Martensitic Transformation in Fe-29.5at.%Ni, *Appl. Phys.*, 1977, **13**, p 105
25. S. Tanigawa, K. Hinode, T. Yamauchi, and M. Doyama, *New Aspects of Maternsitic Transformation*, Japan Institute of Metals, Tokyo, 1976, p 123–128
26. P. Hautojärvi, T. Judin, A. Vehanen, J. Yli-Kauppila, J. Johansson, J. Verdone, and P. Moser, Annealing of Vacancies in Electron-Irradiated α-Iron, *Solid State Commun.*, 1979, **29**, p 855
27. P. Hautojärvi, J. Johansson, T. Judin, P. Moser, M. Puska, A. Vehanen, and J. Yli-Kauppila, *Proceedings of the Fifth International Conference on Positron Annihilation*, Lake Yamanaka, Japan, 1979, R.R. Hasiguti and K. Fujiwara, Ed. (Sendai, Japan), Japan Institute of Metals, 1979, p 737
28. D. Segers, I. Hurtado, L. Dorikens-Vanpraet, and J. van Humbeeck, Positron Doppler Broadening Measurements in Cu-Al-Ni Based Shape Memory Alloys, *J. Phys. IV*, 1995, **5**, p C1–C163
29. D. Segers, J. Van Humbeeck, L. Delaey, M. Dorikens, and L. Dorikens, The Study of Defects in Some CuZnAl Alloys, Positron Annihilation, *Proceedings of the Seventh International Conference* (Singapore), World Scientific, 1985, p 880
30. J. Kansy, Microcomputer Program for Analysis of Positron Annihilation Lifetime Spectra, *Nucl. Instrum. Methods*, 1996, **374**, p 235
31. D. Segers, S. Van Petegem, J.F. Loffler, H. Van Swygenhven, W. Wagner, and C. Dauwe, Positron Annihilation Study of Nanocrystalline Iron, *J. Nano Struct. Mater.*, 1999, **12**, p 1059
32. H. Li, D. Dunne, and N. Kennon, Factors Influencing Shape Memory Effect and Phase Transformation Behaviour of Fe-Mn-Si Based Shape Memory Alloys, *Mater. Sci. Eng. A*, 1999, **273–275**, p 517–523
33. B. Bergersen and M.J. Stott, The Effect of Vacancy Formation on the Temperature Dependence of the Positron Lifetime, *Solid State Commun.*, 1969, **7**, p 1203
34. J.M. Campillo Robles and F. Plazaola, Collection of Data on Positron Lifetimes and Vacancy Formation Energies of the Elements of the Periodic Table, *Defect Diffus. Forum*, 2003, **213–215**, p 141
35. R.N. West, Positrons in Solids, in *Topics in Current Physics*, Vol. 12, P. Hautojarvi, Ed., Springer, Berlin, 1979, p 89
36. T.E.M. Staab, R. Krause-Rehberg, and B. Kieback, Review Positron Annihilation in Fine-Grained Materials and Fine Powders—An Application to the Sintering of Metal Powders, *J. Mater. Sci.*, 1999, **34**, p 3833
37. M.J. Puska, P. Lanki, and R.M. Nieminen, Positron Affinities for Elemental Metals, *Phys. Condens. Matter*, 1989, **1**, p 6081
38. Y. Kamimura, T. Tsutsumi, and E. Kuramoto, Calculations of Positron Lifetimes in a Jog and Vacancies on an Edge-Dislocation Line in Fe, *Phys. Rev. B*, 1995, **52**, p 879
39. K.M. Mostafa, J. De Baerdemaeker, P.R. Calvillo, N. Van Caenegem, Y. Houbaert, and D. Segers, A Study of Defects in Iron Based Alloys by Positron Annihilation Techniques, *J. Acta Phys. Polon. A*, 2008, **113–115**, p 1471

40. Y.-K. Park, J.T. Waber, M. Meshii, C.L. Snead Jr., and C.G. Park, Dislocation Studies on Deformed Single Crystals of High-Purity Iron Using Positron Annihilation: Determination of Dislocation Densities, *Phys. Rev. B*, 1986, **34**, p 823
41. I.K. Mackenzie, A. Eady, and R.R. Gingerich, The Interaction Between Positrons and Dislocations in Copper and in an Aluminum Alloy, *Phys. Lett. A*, 1970, **33**, p 279
42. J.H. Yang and M. Wayman, Development of Fe-Based Shape Memory Alloys Associated with Face-Centered Cubic-Hexagonal Close-Packed Martensitic Transformations, *Metall. Trans.*, 1992, **23A**, p 1445–1454
43. K.M. Mostafa, N. Van Caenegem, J. De Baerdemaeker, D. Segers, and Y. Houbaert, Study of Defects and Phase Transformation in a Fe-Mn-Si-Cr-Ni Alloy by Positron Annihilation Method, *Phys. Status Solidi (c)*, 2007, **4–10**, p 3554